DOI 10.1007/s11182-020-01941-8

Russian Physics Journal, Vol. 62, No. 11, March, 2020 (Russian Original No. 11, November, 2019)

CATHODIC ARC EVAPORATION OF POLYCRYSTALLINE SILICON

D. V. Dukhopel'nikov and D. V. Kirillov UDC 537.525

The paper presents the experimental results of silicon cathodic arc evaporation in a continuous mode with the superimposed external arched magnetic field. Volt-ampere characteristics are obtained for arc discharge and the cathode spot velocity is determined at different external magnetic field. It is shown that the erosion rate of the silicon cathode surface depends on the magnetic field. Silicon coatings obtained by using a continuous mode of cathodic arc deposition, demonstrate the silicon droplet diameter ranging from 30 nm to 5 μm. Experiments show a decrease in the droplet number density and the volume fraction in coatings with increasing magnetic field.

Keywords: vacuum arc, silicon, droplets, cathode spot velocity, arched magnetic field, erosion, coating.

INTRODUCTION

Pure silicon and silicon-containing thin films are used in many industries. Amorphous and nanocrystalline thin silicon film is used in the production of solar cells and also in medicine in the capacity of antimicrobial coatings for instruments and implants [1]. Silicon oxide and silicon nitride films are used in microelectronics and in the manufacture of light emitting diodes. The use of silicon coatings is promising in anodes of lithium-ion batteries with a view to increase their capacity and the number of charge-discharge cycles [2]. Silicon oxide is widely used in optics. Silicon-containing ceramics such as Ti–Cr–Si–N, Ti–Al–Si–N, Al–Cr–Si–N is used as wear-resistant coatings for metal cutting tools [3].

The most common method for synthesis of silicon films and silicon compounds is chemical vapor deposition, including liquid-phase epitaxy, sol-gel method, and plasma-enhanced chemical vapor deposition. Silicon films can also be deposited by vacuum magnetron sputtering and ion-beam sputtering [4, 5]. These methods provide a synthesis of dense, high-purity silicon films having good adhesion to the substrate. However, a significant weakness of these methods is low growth rates of coatings. An alternative method of the silicon and silicon-containing coating deposition is cathodic arc evaporation or cathodic arc physical vapor deposition (CAPVD) [6–9]. In this case, an arc discharge occurs on a cold cathode surface. The evaporated cathode material creates a coating of either a pure cathode material or its reactive gas compounds on the parts. This method provides a high density coating, good surface adhesion, high performance and stability. Cathodic arc evaporation is used to deposit protective, decorative, wear-resistant and diamond-like coatings [10, 11].

Research into cathodic arc deposition of silicon films usually concerns pulsed [12] or periodic [13] discharges, which are not effective enough for industrial applications. Thermal deformation of the silicon cathode occurs during continuous cathodic arc evaporation due to a non-uniform power distribution by the slow-moving cathode spot. This can be avoided by either the forced motion of cathode spots over the cathode surface [7, 8] or using a periodic operation mode [13].

Bauman Moscow State Technical University, Moscow, Russia, e-mail: duh@bmstu.ru; kirillovdv@bmstu.ru.
Translated from Izvestiya Vysshikh Uchebnykh Zavedenii, Fizika, No. 11, pp. 68–74, November, 2019. Original article submitted September 13, 2019.

In our former research [6], silicon cathodic arc evaporation was conducted in the continuous, prolonged mode with the external arched magnetic field. Cathode spots moved along a closed path determined by the configuration of the magnetic system, at a speed proportional to the tangent component of the magnetic field, which provided a uniform power delivery to the active cathode surface. Such an evaporation technique of pure silicon, silicon alloys or a combination of other materials (titanium, aluminum, chromium) allowed us to carry out vacuum deposition of dense silicon or silicon-containing coatings without the cathode disintegration caused by thermal deformation, while also maintaining high performance and simultaneous reduction in the number of droplets in erosion products.

The work [6] showed the synthesis of smooth, homogeneous silicon coatings with satisfactory adhesion using the CAPVD technique. The number and the size of droplets is one of the important characteristics of CAPVD coatings. It was found that the size of silicon droplets in CAPVD coatings ranged from 30 nm to 5 μm. The droplets were flat and toroid. For most droplets, the ratio between the droplet height and diameter ranged between 0.02 and 0.08. Flat shape of the silicon droplets indicated that they appear on the substrate surface in a liquid state regardless of size.

There is virtually no information offered in the literature concerning the properties of CAPVD with use of silicon, in presence of the external arched magnetic field. Little is known at present about the silicon erosion products, in particular, liquid droplets depositing on the substrate and causing the surface defects. This paper discusses these issues.

MATERIALS AND METHODS

A vacuum arc evaporator with cathode diameter of 150 mm was used in this experiment [6]. Polycrystalline silicon (90%) and aluminum (10%) alloy plate 8 mm thick was soldered to a copper base and used as a cathode material. The discharge current varied from 40 to 120 A at 19–26 V. An electromagnetic system was used to create an arched vacuum magnetic field. This provided a circular motion of cathode spots at an increased velocity. The circle radius was determined by the current ratio in magnetic coils of the vacuum arc evaporator. The magnetic field ranged from 2.5 to 11 mT at the arch center, where the cathode spot motion occurred. The operation of the vacuum arc evaporator at a lower magnetic field was not considered here, because at a low velocity of the cathode spot, the cathode could disintegrate due to its overheating. An EWM Tetrix 230 AC/DC welding system (Austria) was used as a power source. The discharge was initiated by plasma injection into the interelectrode gap.

Photographic recording was used to measure the cathode spot velocity. A VS-FAST NG high-speed camera (OOO “Videoscan”, Russia) was installed in front of the end of the vacuum arc evaporator, normal to the cathode surface. The cathode spot velocity was calculated from the obtained path length and the exposure time.

The erosion rate was determined by direct cathode weighing after 5 min of continuous operation at a 100 A current and 2.5–12.5 mT magnetic field. The cathode was weighted on Sartorius™ Cubis™ MSE Analytical Balances (Germany) with 1 mg readability.

The composition of the dispersed phase was investigated on the deposited coatings. The coatings were deposited onto 30×40×3 mm substrates made of the grade M1 float glass. The distance to the cathode was 240 mm; the substrates were placed perpendicular to the plasma flow. The deposition time of 15 s was determined by the following criteria: 1) the substrate surface must have enough droplets for analysis; 2) the droplets must not overlap; 3) the droplets must not be completely embedded in the growing film. In these conditions, the coating thickness ranged from 20 to 35 nm. An atomic force microscope (AFM) MultiMode 8 (Bruker, USA) and a confocal laser scanning microscope (CLSM) Zeiss LSM 700 (Germany) were used to measure the droplet size. According to the AFM and CLSM images given in Fig. 1, it ranged between 0.01–1.00 μm and 1–10 μm, respectively. To cover the full range of the droplet size, we obtained a number of images with different resolutions. The AFM images clearly display the uniform coating, without an islet structure.

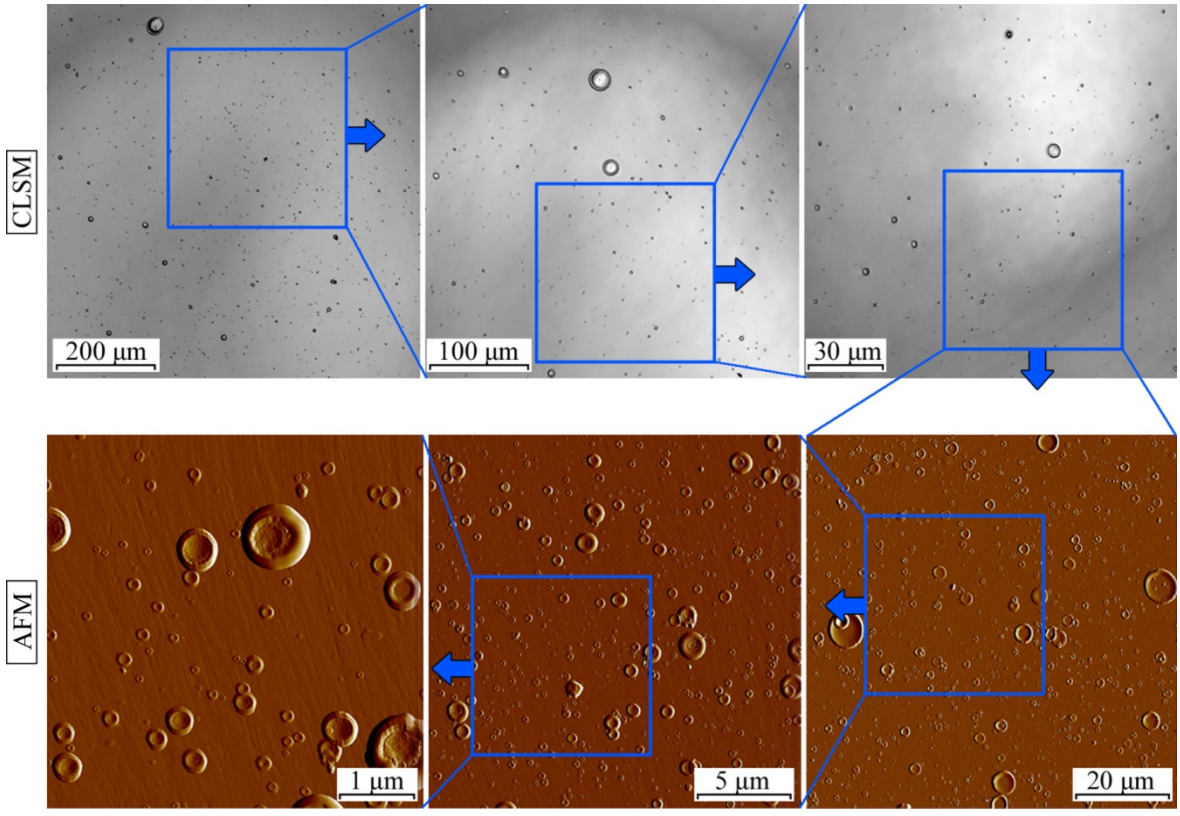

Fig. 1. CLSM and AFM images with different resolutions. Magnified regions are conventional. Silicon deposition time: 15 s.

RESULTS AND DISCUSSION

In CAPVD, plasma ionization achieves 100%, and even weak magnetic fields of about 0.2 mT can have a noticeable effect on volt-ampere characteristics (VAC) of the arc discharge. Also, an increase in the discharge voltage provides the electron temperature rise and contributes to the additional plasma heating. The resulting VAC of the arc discharge on the silicon cathode is similar to that on a metal cathode surface, *i.e.* VAC is growing. As can be seen from Fig. 2, the increase in the magnetic field from 2 to 13 mT causes the discharge voltage growth from 19 to 25 V. The increase in the discharge voltage occurs due to a voltage drop in the cathode region, which, in turn, results from the decrease in the plasma conductivity across the magnetic field lines.

As presented in Fig. 3, the increase in the magnetic field from 2 to 12 mT promotes the increase in the cathode spot velocity from 2 to 4.5 m/s over the cathode surface, at a 100 A discharge current. The path of cathode spot motion over the cathode surface in the arched magnetic field represents a broken curve passing through the arch center. With increasing magnetic field the broken line straightens, thereby increasing the cathode spot velocity. The limit value of the velocity increase corresponds to the completely straightened curve.

The cathode erosion rate of the arc evaporator is calculated from the mass difference Δm before and after the continuous cathodic arc evaporation process [14]:

$$E_r = \frac{\Delta m}{I_d t}, \quad (1)$$

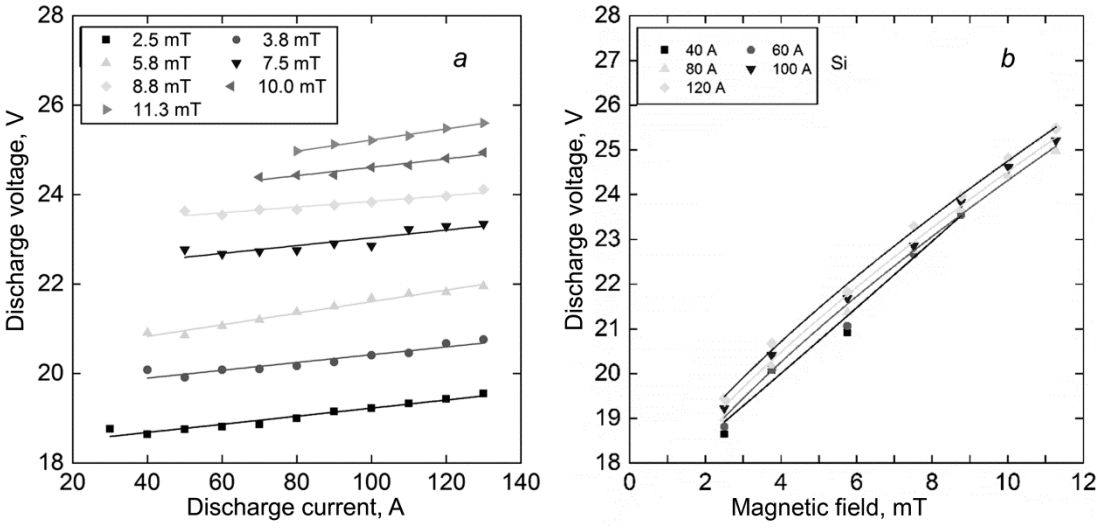

Fig. 2. Magnetic field and VAC dependence of the arc discharge on silicon cathode surface.

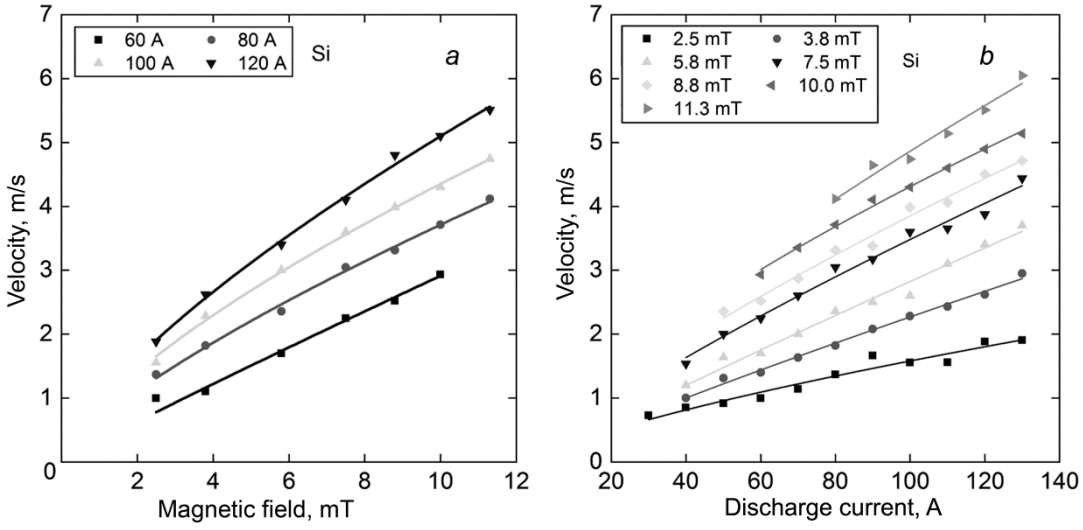

Fig. 3. Dependence of magnetic field and discharge current on the cathode spot velocity.

where Δm is the loss in the cathode weight, kg; t is the time of continuous operation, s; I_d is the discharge current, A.

Figure 4 plots the dependence between the magnetic field and the rate of the cathode erosion. According to this figure, the erosion rate decreases, when the magnetic field lowers. The erosion rate of silicon is 1.5 times higher than that of titanium and almost matches that of aluminum. The decrease in the erosion rate may be caused by the reduced emission of ions, droplets or neutral atoms from the cathode spot crater.

Until recently, the effect of the erosion rate reduction in the arched magnetic field was neglected in design of arc evaporators. However, at 4 mT and higher magnetic field the above data illustrate that the reduction in the erosion rate can be significant.

Data on the droplet (macroparticle) size on the substrate are obtained at a 100 A discharge current and with three values of magnetic field, *viz*. 2.5, 6.25 and 12.5 mT. The average size of droplets is measured for each mode using two or three thousand droplets. Bar diagrams given in Fig. 5 describe the density of the droplet flow onto the substrate and are obtained as

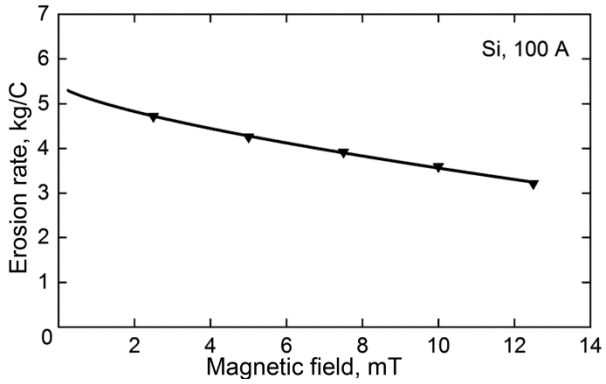

Fig. 4. Dependence between the magnetic field and the rate of Si cathode erosion.

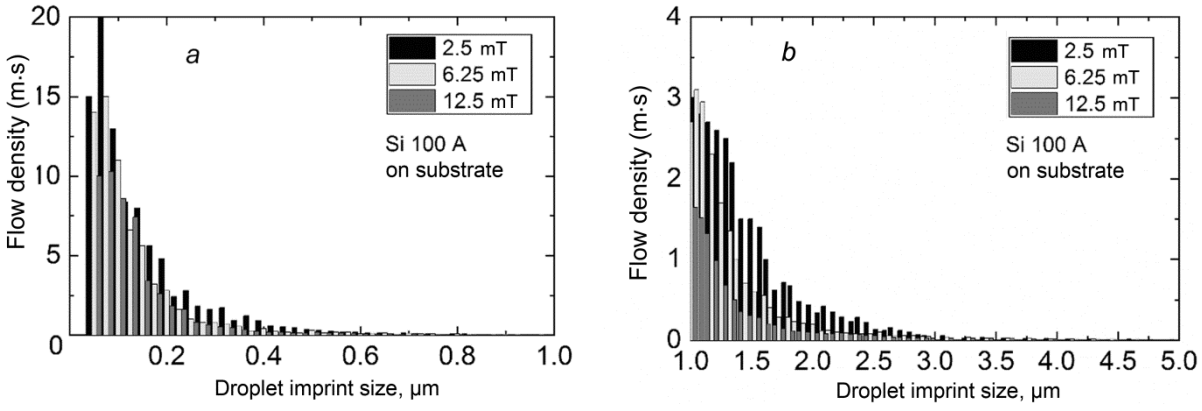

Fig. 5. Bar diagrams of the number of droplets deposited onto the substrate area.

$$\dot{n} = \frac{n_a}{S \cdot t}, \tag{2}$$

where n_a is the number of droplets deposited onto the substrate area S during the time t.

According to Fig. 5, which gives the data on the size range of 0–1 μm (*a*) and 1–5 μm (*b*), the number of droplets on the substrate lowers by 1.5–2 times in superimposing the magnetic field, due to the great difference in the flow density, which proves the results obtained in [15].

In our earlier research [6], the droplets depositing on the substrate are liquid and deform after collision with the substrate. The size of the droplet imprint is 2.5–3.5 times larger than its diameter before collision. Subsequent calculations of the distribution functions of the droplet diameter and weight fraction are performed for droplets before collision with the substrate. And the droplet size is recalculated accordingly.

The size of droplets that carry most of the flow mass is determined by the function $f_m(a)$ of mass distribution between the droplet fractions, which is plotted in Fig. 6:

$$f_m(a) = \frac{1}{m_\Sigma}\frac{\Delta m(a)}{\Delta a} = \frac{1}{n\int f(a)m(a)da}\frac{m(a)\Delta n(a)}{\Delta a} = \frac{m(a)f(a)}{\int f(a)m(a)da}, \tag{3}$$

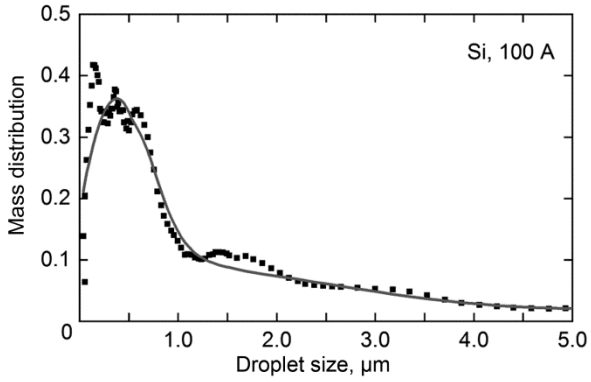

Fig. 6. Function of mass distribution between droplet fractions.

where $\Delta m(a)$ is the mass fraction m in the flow of droplets with the size of $a \pm \Delta a$, m_Σ is the total mass of droplets.

The imprint diameter distribution function $f(a)$ is the probability of detecting the value a in the range Δa, which is calculated as

$$f(a) = \frac{1}{\dot{n}} f^*(a_i) \approx \frac{1}{\dot{n}} \frac{\Delta \dot{n}_{at}}{\Delta a_i} \ , \tag{4}$$

if the range of droplet imprints is minimum. We assume that $\Delta a_i = 25$ nm. The flow density $\Delta \dot{n}_{at}$ in the indicated range is obtained from measurement results. The function $f^*(a_i)$ is an unnormalized function of the size distribution.

The total droplet number $\dot{n}$ can be obtained using the following condition:

$$\frac{1}{\dot{n}} \int f^*(a)\, da = \int f(a)\, da = 1 . \tag{5}$$

Hence, $\dot{n}$ value is determined as

$$\dot{n} = \int f^*(a)\, da \tag{6}$$

and found directly from the experimental data.

Based on $f_m(a)$ function, it is found that 70% of the mass flow carried by the droplet phase falls on droplets with the size varying from 0 to 1.1 μm; the size of imprints on the substrate varies from 0 to 2.8 μm. Thus, the mass fraction of droplets in plasma can be decreased *via* the reduction of the number of droplets within this size range.

In order to quantify the reduction in the droplet number, the droplet mass fraction γ_m is calculated in coatings at different values of magnetic field:

$$\gamma_m = \frac{m_\mathrm{d} / S}{m_\mathrm{d} / S + m_\mathrm{c} / S} , \tag{7}$$

where m_d / S is the droplet mass in the coating with the area S, m_c / S is the coating mass per area S.

The value of m_d / S is estimated by measuring the coating thickness in an area without droplets. The droplet mass is found from

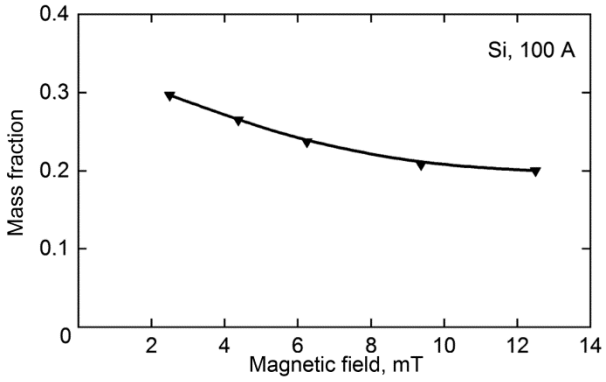

Fig. 7. Dependence between magnetic field and droplet mass fraction in the silicon coating.

$$\frac{m_{\mathrm{d}}}{S} = n_{\mathrm{d}} \int n(a) m(a)\, da = \frac{\pi}{4} n_{\mathrm{d}} \rho \int f(a) a^3 A(a)\, da\,. \tag{8}$$

The mass fraction of droplets is calculated for different values of the magnetic field at a 100 A discharge current. In Fig. 7 one can see that the droplet mass fraction in the silicon coating ranges between 0.20 and 0.30. And the increase in the magnetic field decreases the mass fraction of silicon droplets in the vacuum arc discharge by 1.5 times.

CONCLUSIONS

The application of the arched magnetic field provided the increase in the velocity of cathode spots and their path control. This promoted the evaporation of fragile semiconductor materials, including silicon, and the synthesis of silicon coatings with the reduced number of droplets.

It was shown that the arched magnetic field reduced the droplet flow density by 1.5–2 times and the mass fraction in coatings, which varied between 0.2 and 0.3, depending on the magnetic field values.

The VAC of the arc discharge on the silicon cathode with the arched magnetic field was growing, and at a discharge current of 100 A, the magnetic field increased from 2.5 to 12 mT resulted in the discharge voltage growth from 19 to 25 V.

The increase in the magnetic field from 2.5 to 12 mT led to the erosion rate reduction from $4.7 \cdot 10^{-8}$ to $3.2 \cdot 10^{-8}$ kg/C.

REFERENCES

1. M. S. Laranjeira, A. Carvalho, A. Pelaez-Vargas, *et al*., Sci. Technol. Adv. Mater., **15**, No. 2, 025001 (2014). DOI: 10.1088/1468-6996/15/2/025001.
2. M. Ge, X. Fang, and J. Rong, Nanotechnology, **24**, No. 42, 422001 (2013). DOI: 10.1088/0957-4484/24/42/422001.
3. N. A. Timchenko, Y. V. Zubavichus, and O. V. Krysina, J. Surf. Investig., **10**, No. 2, 425–428 (2016). DOI: 10.1134/S1027451016020373.
4. V. M. Sharapov, A. M. Zimin, S. E. Krivitsky, *et al*., J. Surf. Invest.: X-ray, Synchr. Neutr. Techn., **9**, No. 4, 673–678 (2015). DOI: 10.1134/S1027451015040187.
5. D. V. Dukhopel'nikov, V. S. Bulychev, and E. V. Vorob'ev, Vestnik Moskovskogo gosudarstvennogo tekhnicheskogo universiteta im. N. E. Baumana. Ser. Estestvennye nauki, **76**, No. 1, 95–103 (2018).

6. D. V. Dukhopel'nikov, D. V. Kirillov, and V. S. Bulychev, Vse materialy. Entsiklopedicheskii spravochnik, No. 12, 18–24 (2015).
7. D. V. Dukhopel'nikov, A. V. Zhukov, D. V. Kirillov, *et al*., Meas. Tech., No. 10, 995-999 (2005).
8. A. I. Ryabchikov, D. O. Sivin, P. S. Ananin, *et al*., J. Ind. Pollut. Control, **32**, No. 2, 406–410 (2016).
9. B. A. Timerkaev and A. A. Andreeva, J. Phys.: Conf. Ser., **1058**, No. 1, 012071 (2018). DOI: 10.1088/1742-6596/1058/1/012071.
10. Y. M. Mironov, R. O. Stepanov, A. S. Osipkov, *et al*., in: Proc. 5th Int. Workshop on Computer Science and Engineering: Information Processing and Control Engineering, Moscow (2015).
11. A. S. Osipkov, V. M. Bashkov, A. O. Belyaeva, *et al*., IOP Conf. Ser.: Mater. Sci. Eng., **74**, No. 1, 012013 (2015). DOI: 10.1088/1757-899X/74/1/012013.
12. A. Anders and G. Yu. Yushkov, J. Appl. Phys., **91**, No. 8, 4824–4832 (2002). DOI: 10.1063/1.1459619.
13. R. K. Tripathi, O. S. Panwar, and I. Rawal, J. Taiwan Inst. Chem. E., **86**, 185–191 (2018). DOI: 10.1016/j.jtice.2018.01.051.
14. J. E. Daalder, J. Phys. D: Appl. Phys., **8**, No. 14, 1647–1659 (1975). DOI: 10.1088/0022-3727/8/14/009.
15. P. D. Swift, J. Phys. D: Appl. Phys., **29**, No. 7, 2025–2031 (1996). DOI: 10.1088/0022-3727/29/7/041.